# Effects of gold patterning on the bending profile and frequency response of a microcantilever

Dongkyu Lee,[1] Seonghwan Kim,[2] Namchul Jung,[1] Thomas Thundat,[2] and Sangmin Jeon[1,a)]
[1]*Department of Chemical Engineering, Pohang University of Science and Technology, Pohang, Kyungpook 790-784, Republic of Korea*
[2]*Biosciences Division, Oak Ridge National Laboratory, Oak Ridge, Tennessee 37831, USA*

(Received 27 May 2009; accepted 19 June 2009; published online 27 July 2009)

We have systematically investigated the effect of various gold patterns on the bending profile and frequency response of a microcantilever. The gold patterns were deposited on the cantilever arrays using four types of shadow mask. The local bending profile, slope, and curvature varied depending on the area and position of the gold pattern. Also, the variations in the first three modes of the flexural resonance frequencies of the gold patterned cantilevers were measured to understand the opposing effects of mass loading and flexural rigidity; both of these parameters are dependent on the position and area of the gold pattern. The experimental results validated the theoretical one-dimensional model introduced by Tamayo *et al.* [Appl. Phys. Lett. **89**, 224104 (2006)] and our calculations using the finite element method. The gold patterns giving the maximum response of the mass loading and flexural rigidity change were determined by examining how the relative resonance frequency shifts as a function of the distance of the gold coating from the free end or clamping region. The results of this study can potentially be applied in the design of a microcantilever sensor in which pattern analysis is utilized to determine the presence of adsorbed biological and chemical molecules. © *2009 American Institute of Physics*. [DOI: 10.1063/1.3177326]

## I. INTRODUCTION

Microcantilevers have been widely used as highly sensitive sensor platforms for the label-free detection of chemical and biological analytes.[1–4] Microcantilever sensors have two operational modes: the static mode and dynamic mode. The static mode measures the variation in the deflection of a cantilever due to adsorption-induced surface stress changes, while the dynamic mode measures the variation in the resonance frequency of a cantilever due to adsorption-induced mass or stiffness changes.[5,6]

The mass adsorbed on a microcantilever generally decreases the resonance frequency when the adsorbed mass is uniformly distributed. However, in spite of adding mass to the microcantilever, the resonance frequency often increases due to surface stress-induced changes in the spring constant.[7] Recently, Ramos *et al.*[8–10] and Tamayo *et al.*[11] demonstrated that the position and stiffness of adsorbed *Escherichia coli* bacteria on a cantilever affect the resonance frequency shifts. The frequency response of a microcantilever depends not only on the position of the added mass but also on the flexural rigidity change that results from the position and stiffness of the adsorbate.

The deflection of cantilevers has been used for highly sensitive and selective measurements of thiol self-assembled monolayers and biomolecules.[12,13] A thin gold film is typically coated on one side of the microcantilever in order to selectively functionalize the surface of the cantilever with thiol compounds. However, the gold coating produces significant residual stress that affects the sensitivity and reproducibility of the cantilever's response to molecular adsorption.[14] Several studies[14–16] have investigated the origin of variation in the surface stress of fully gold-coated cantilevers along with the sensitivity and reproducibility of their static response to molecular adsorption. However, a detailed systematic study of partially gold-coated cantilevers has not been performed and is needed to completely understand the variation in the deflection of cantilevers.

Single optical beam deflection systems have generally been employed to measure the variation in the deflection of the cantilever's end position assuming constant bending in Stoney's equation. However, deviation from a constant radius of curvature can occur during the adsorption process on the cantilever. As a result, the bending profile of a cantilever has recently been measured in order to fully understand surface stress-induced changes in curvature using several methods such as multiple-point laser signal transductions,[17] profilometers,[18] and interferometry.[19] Although the bending profile of a partially coated cantilever has been captured and analyzed to determine how the adsorbate position influences local changes in curvature,[9] the effects of the adsorbate position on the cantilever bending profile still need to be systematically investigated. Unfortunately, a recent related study that focused on the adsorption of *E. coli* bacteria reported large uncertainties for important parameters such as the elastic modulus, added mass, and coated area.

Here, we describe a more reliable and systematic method to fully understand how the cantilever bending profiles and frequency responses vary with the position of adsorbate and the extent of adsorption. The gold patterns were deposited on the cantilevers using four types of shadow mask. The thin gold film on the microcantilevers induced tensile stress due

a)Electronic mail: jeons@postech.ac.kr.

 

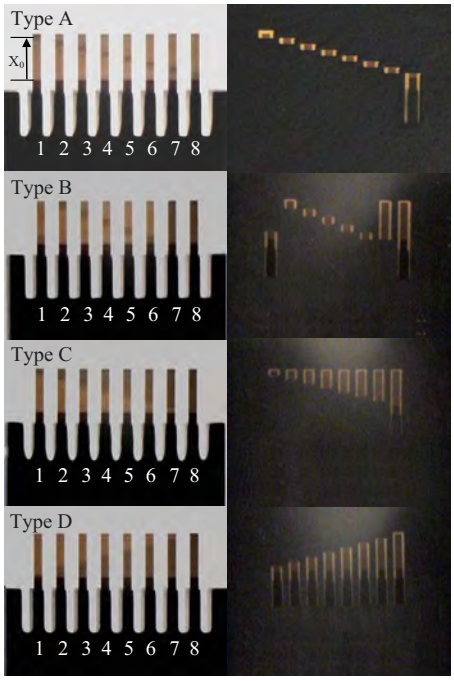


FIG. 1. (Color online) Optical images of gold patterned cantilever arrays and types A–D shadow masks: the partially coated cantilevers with 100 $\times 62.5$ $\mu m^2$ (type A) and $100 \times 100$ $\mu m^2$ (type B) gold patterns, the gold patterned cantilevers with a 62.5 $\mu$m stepwise increases in the distance from the free end region (type C) or from the clamping region (type D).

to residual surface stress. Variations in the position and area of the gold film on the microcantilevers resulted in different bending profiles. The resonance frequency was measured by recording the frequency spectrum of acoustically actuated cantilevers in dry nitrogen. Variations in the first three modes of flexural resonance frequencies were determined for the gold patterned cantilevers. The experimental results verified the theoretical one-dimensional model of Tamayo and co-workers[8–11] as well as our computational calculations using the finite element method (FEM). The conditions that resulted in the largest response in mass loading and flexural rigidity change were determined by examining the relative resonance frequency shifts as a function of gold coating distance from the free end or clamping region.

## II. MATERIALS AND METHODS

### A. Preparation of gold patterned microcantilevers

We used commercially available arrays of eight silicon cantilevers. The cantilever arrays were purchased from Concentris (Basel, Switzerland). Each cantilever in the array was 500 $\mu$m long, 100 $\mu$m wide, and 1 $\mu$m thick, and had a spring constant of $\sim 0.026$ N/m. The shadow metal masks used for the gold patterns were obtained from ALTUS Inc. (Yongin, Korea). Figure 1 shows the optical images of four representative gold patterned cantilevers (left column) and the corresponding masks on the cantilever arrays (right column). The size and position of the gold pattern on each set of cantilevers were similar to those on the corresponding mask within $\pm 4$ to 5 $\mu$m. Four different masks (types A–D) were used to deposit different gold pattern sizes at various positions along the length of the cantilevers. As is shown in Fig. 1, 500 $\mu$m long cantilevers were divided into eight regions for type A and five regions for type B. The gold pattern sizes were $100 \times 62.5$ $\mu m^2$ for type A and $100 \times 100$ $\mu m^2$ for type B. The longitudinal center ($X_0$) distances from the clamping region were 468, 406, 343, 281, 218, 156, 93, and 31 $\mu$m for cantilevers 1–8 in type A, respectively. For type B, $X_0$ was 50, 450, 350, 250, and 150 $\mu$m for cantilevers 1–5, respectively. In comparison with the cantilevers 1 and 8, the gold patterns on cantilevers 6 and 7 in type B were originally designed to study the difference between cantilevers with and without gold coating extending to the clamping region; however, due to unsuccessful confinement of the gold coating to the clamping region, the experiments could not be performed and hence no data are presented for these cantilevers. Types C and D produced gold patterns that were systematically increased stepwise by 62.5 $\mu$m from the free end region and clamping region.

Each cantilever array was coated with 3 nm of titanium followed by 20 nm of gold at a deposition rate of 0.05 nm/s; the metal layers were deposited through the shadow masks by thermal evaporation. The coating thickness of the cantilevers was determined with an atomic force microscope (Veeco, Santa Barbara, CA).

### B. Measurement of the bending profile and the resonance frequency

Bending profiles of each cantilever array before and after gold coating were measured using a Wyko NT1100 optical surface profiler (Veeco, Santa Barbara, CA) that utilizes white light interferometry for high resolution three-dimensional (3D) surface measurements. The bending profile measurements were performed at a constant temperature of 20 °C, which was maintained using a Peltier thermoelectric system.

The resonant frequency of an acoustically excited cantilever was measured with a spectrum analyzing LABVIEW program and data acquisition board (National Instruments, Austin, Texas) connected to a multimode atomic force microscopy head (Veeco, Santa Barbara, CA). The acoustic excitation was supplied by the piezoelectric metal holder actuated by a function generator (Stanford Research Systems, Sunnyvale, CA, USA). The relative humidity was maintained below 1% by using dry nitrogen during the measurement and was monitored using a commercial moisture sensor (Picotech, Cambridgeshire, U.K.). The resonance frequencies of the cantilevers were measured at room temperature. We found that the resonance frequencies were almost constant when the cantilever was heated from room temperature to 100 °C.

### C. Theoretical and computational calculation of the resonance frequency of a gold patterned microcantilever

To understand the effect of gold patterning on the frequency response of a microcantilever, the differential Euler–Bernoulli beam equation modified to accommodate the par-

tial gold coating was employed.[8–11] The differential equation of the vibration is given by

$$\frac{\partial^2}{\partial x^2}\left[D(x)\frac{\partial^2 u(x,t)}{\partial x^2}\right] + W[\rho_c T_c + \rho_g T_g(x)]\frac{\partial^2 u(x,t)}{\partial t^2} = 0, \quad (1)$$

where $u(x,t)$ is the flexural displacement, $x$ is the spatial coordinate along the cantilever, $t$ is time, $W$ is the width of the cantilever, $\rho_c$ and $T_c$ are the mass density and thickness of the cantilever, $\rho_g$ and $T_g$ are the mass density and thickness of the gold film on the cantilever, and $D(x)$ is the cantilever flexural rigidity given by

$$D(x) = \frac{W}{12}\frac{E_c^2 T_c^4 + E_g^2 T_g^4(x) + 2E_c E_g T_c T_g(x)[2T_c^2 + 2T_g^2(x) + 3T_c T_g(x)]}{E_c T_c + E_g T_g(x)}, \quad (2)$$

where $E_c$ and $E_g$ are the Young's moduli of the cantilever and gold film, respectively. By applying Rayleigh's method, the resonance frequency is obtained as[8–11]

$$\omega_n^2 = \frac{\int_0^L D(x)\left(\frac{d^2\psi_n(x)}{dx^2}\right)^2 dx}{\rho_c W T_c \int_0^L \left(1 + \frac{\rho_g}{\rho_c}\frac{T_g(x)}{T_c}\right)\psi_n^2(x)dx}, \quad (3)$$

where $\omega_n$ is the $n$th mode angular resonance frequency, $L$ is the length of the cantilever, and $\psi_n$ is the $n$th flexural vibration mode shape of the unloaded cantilever.

The cantilever structures were simulated with finite element software (COMSOL MULTIPHYSICS). The dimensions of the cantilevers and gold patterns used in the simulation were the same as those used in the experiments. The mesh of two-dimensional analysis consisted of $1\times1$ $\mu m^2$ squares. Air-structure interactions were not considered.

The relative frequency shift in each resonant mode was calculated by dividing the $n$th mode resonance frequency shift $(\omega_n - \omega_{n,0})$ by the $n$th mode resonance frequency of the bare silicon cantilever $\omega_{n,0}$.

## III. RESULTS AND DISCUSSION

### A. Bending profiles of gold patterned microcantilevers

White light interferometry was used to characterize the bending profiles of the cantilever arrays with various gold patterns. Figure 2 shows the reconstructed 3D profiles and interference fringes for the different types of cantilever array. The bending profiles of the silicon cantilevers were also measured before the gold coating was added. The intrinsic deflection of the uncoated silicon cantilevers was less than 80 nm and the deviation in deflection for each cantilever in the array was less than 50 nm. This indicates that the 3D profiles for types A–D represent actual cantilever bending that is induced by the residual stress of gold film deposited on the cantilevers. The interference fringes shown on the right of Fig. 2 correspond to the 3D profiles on the left of the figure. Clear and dense interference fringe patterns were observed at the sharp bending area of the gold patterned cantilevers. The gold patterned cantilevers bent upward due to the residual tensile stress of the gold film. The residual tensile stress is related to the nanostructure of the gold film and the formation of well-defined grain boundaries. The grain boundaries that are formed at the expense of strain energy in the grains induce a large tensile stress upon the cantilever.[14] The upward bending displacement of the fully coated cantilever in each array was about 5 to 6.5 $\mu$m. The overall difference in displacement was within 1.5 $\mu$m and is presumably due to intrinsic variations in each array. To normalize the bending profiles, each deflection of partially gold coated cantilevers was divided by the maximum deflection of the fully coated cantilever in each array. For type A, which did not include the fully gold coated cantilever, the bending profiles were normalized by the total sum of maximum deflections in cantilevers 1–8.

Figures 3(a) and 3(b) show the normalized bending profiles for type A ($100\times62.5$ $\mu m^2$) and type B ($100\times100$ $\mu m^2$). The partially coated cantilevers bent upward at the beginning of the gold films and different bending profiles

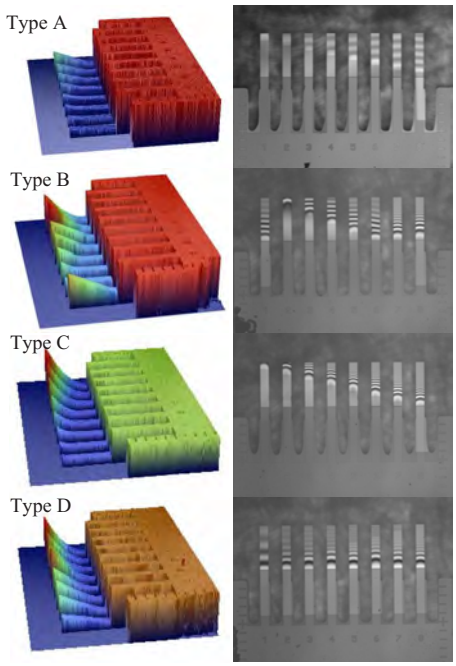


FIG. 2. (Color online) Reconstructed 3D profile images and interference fringes of types A–D.

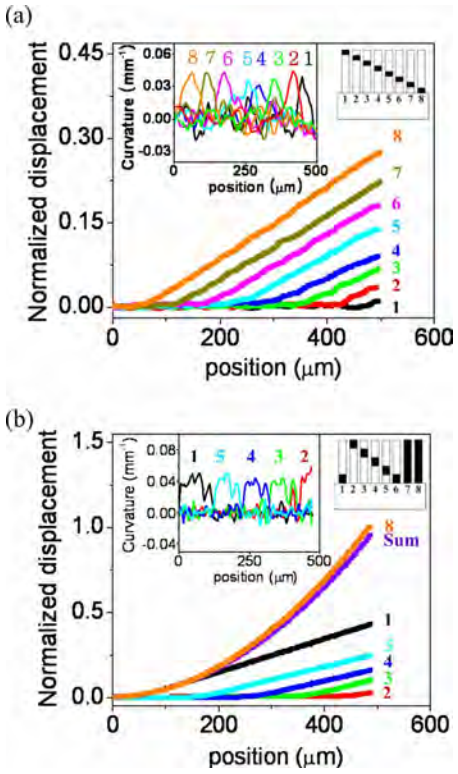


FIG. 3. (Color online) Bending profiles for types A and B cantilevers: the insets show the local curvatures derived from the cantilever profiles in types A and B, respectively.

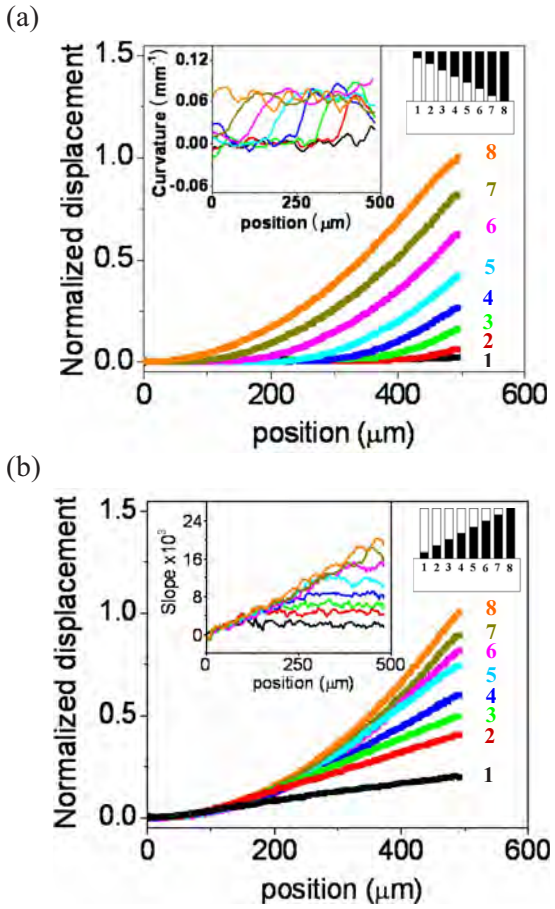


FIG. 4. (Color online) Bending profiles of types C and D cantilevers: the insets of (a) and (b) show the local curvatures of the cantilevers in type C and the bending slopes of the cantilevers in type D, respectively.

of cantilevers were observed for different positions and areas of the partial gold coating. The bending profiles of type A cantilevers 1–8 [Fig. 3(a)] show parallel bending profiles from the end of each gold coated region. This bending profile is due to each gold coated region having approximately the same local curvature coupled to nonbending of the free ends of the cantilevers. The similar bending profile was clearly observed for type B cantilevers 1–5 [Fig. 3(b)] but with larger deflection due to greater local bending curvature that is induced by the larger gold coating areas. In addition, this verifies that the same local curvature is induced by the same area of gold coating because the sum of each bending profile for cantilevers 1–5 is similar to the bending profile for the fully gold-coated cantilever (cantilever 8).

The insets of Figs. 3(a) and 3(b) show the local curvatures derived from the cantilever profiles in types A and B respectively. The curvature $(1/R)$ and the slope can be approximately defined as second and first derivatives of the cantilever profiles with respect to the position of the cantilever. The local curvatures were $\sim 0.05$ $\mathrm{mm}^{-1}$ at gold-coated areas, which is similar to the curvature observed for the fully gold-coated cantilever. The curvature of the uncoated silicon area was zero because the slope of the uncoated silicon area was zero or constant. These results imply that the position and area of the gold patterns on the cantilevers can be determined by all of the following: the bending profiles, changes in the bending slope, and the local curvature.

In order to understand how the bending profiles of cantilevers are affected by the area of the gold pattern, types C and D cantilevers were prepared (Fig. 1). Figures 4(a) and 4(b) show the bending profiles of gold patterned cantilevers having a 62.5 $\mu$m stepwise increase in the distance from the free end and clamping region, respectively. The deflection of types C and D cantilevers gradually increased as the gold coating area increased and the bending profiles of the partially coated cantilevers approached the bending profile of the fully gold coated cantilever (cantilever 8). As is demonstrated in Fig. 4(a), the gold films on the type C cantilevers changed the local bending profile of the cantilevers at the gold coated regions. The bending profile of the cantilevers clearly showed the local curvature at the gold coated areas. Each type D cantilever in Fig. 4(b) showed local bending curvature at the gold coated regions and a tangent line at the end of the gold coated region.

Although it is difficult to identify the gold coated regions on the cantilevers from the bending profiles in Fig. 4(b), the gold coated region on each cantilever can be clearly determined from the slope of the profile [Fig. 4(b), inset]. The slopes of the gold coated regions continually increase, whereas those for the uncoated silicon region are nearly constant. This indicates that the bending slope of the uncoated silicon region in type D is determined by the gold coating length. The above results imply that the bending magnitude of a partially coated cantilever can be controlled by both the coating position and the coating area.

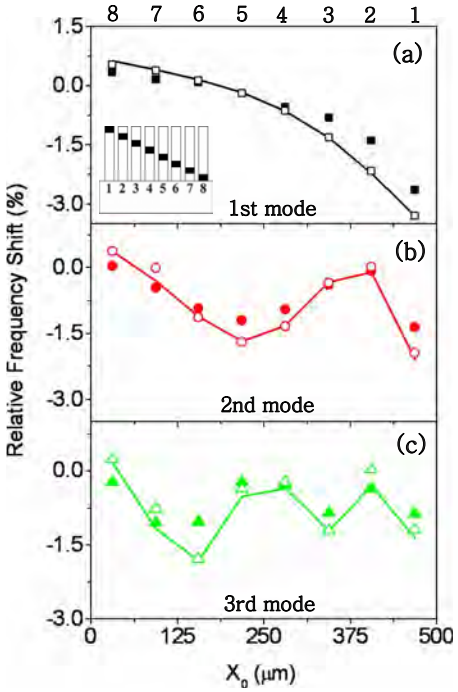


FIG. 5. (Color online) The effect of gold coating position on the first three modes of the flexural resonance frequency shifts for the type A cantilever array as a function of the center position ($X_0$) of the gold rectangles: (a) first (black squares), (b) second (red circles), and (c) third (green triangles). The solid symbols represent the experimental data. The open symbols and the colored lines represent FEM simulation results and theoretical calculations, respectively. The relative frequency shifts for each resonant mode are the percentage of the resonance frequency shift divided by the *n*th mode resonance frequency.

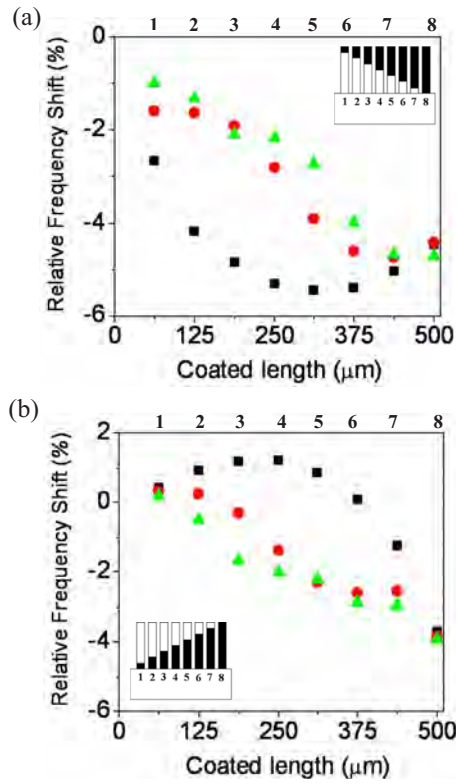


FIG. 6. (Color online) Relative frequency shifts for the first three modes as a function of the coating distance from the (a) free end and (b) clamping region: first (black solid squares), second (red solid circles), and third (green solid triangles).

### B. Frequency responses of gold patterned cantilevers

Figure 5 shows the effect of the gold coating position on the first three modes of flexural resonance frequencies for the type A cantilever array (cantilevers 1–8). The quality factors of the cantilevers were slightly increased after the gold coating due to the increase in the total vibrational energy.[20] We compared the experimental data to theoretical predictions and FEM calculations. The symbols and lines represent the experimental data (solid symbols), simulation results (open symbols), and theoretical values (lines) of the relative frequency shifts for the first three resonant modes. The theoretical predictions and FEM results provide trend curves that correspond well with the experimental data. This indicates that the theoretical one-dimensional model developed by Tamayo and co-workers and FEM analysis can be used to predict the present experimental data, although slight deviations in the magnitude of the frequency shifts are still observed. The discrepancy in Fig. 5 can be explained by the following: (1) the theoretical model and FEM calculations do not take into account environmental and internal damping of cantilever vibrations and (2) the assumed vibration shapes of a cantilever in the one-dimensional model and FEM calculations are different from those for a gold patterned cantilever.

The mass and flexural rigidity have opposite effects on the resonance frequency shifts.[7] In Fig. 5, the gold patterns near the free end region on cantilever 1 caused a decrease in frequency due to the increase in mass, while the gold patterns near the clamp region on cantilever 8 caused an increase in frequency due to an increase in flexural rigidity. The relative resonance frequency shifts of the fundamental mode for the cantilevers in Fig. 5(a) are generally greater than the others because the vibration shapes of a cantilever in higher modes [Figs. 5(b) and 5(c)] have nodes and antinodes that weaken the mass and rigidity effects. The local maxima and minima of the relative frequency shifts are related to the positions of the nodes and antinodes. Thus, the positions of the nodes and antinodes can be resolved by analyzing the frequency responses of a finely patterned cantilever. In addition, positions that induce zero frequency shifts in various vibration modes are observed in Fig. 5. Figures 5(b) and 5(c) display the multiple zero crossover positions of the higher modes that are induced by the gold coating on the nodes. The coating positions induce positive frequency shifts only when they are located near the clamping region because the rigidity effect at the clamping region is higher than the mass effect; the rigidity effect at the other nodes is cancelled by the mass effect. The crossover positions of the first mode near the clamping region are $\sim 190$ $\mu$m. Thus, the flexural rigidity effect is the same as the mass effect at $X_0 = \sim 0.38$ L for the first mode.

To understand the positive frequency shifts in cantilevers coated near the clamping areas, the frequency shifts in types C and D cantilever arrays were measured. Figure 6 shows the relative frequency shifts in the first three modes for types C and D. As shown in Fig. 6, the minima and maxima of the fundamental resonance frequency shift are observed for different coating lengths because the mass competes with the

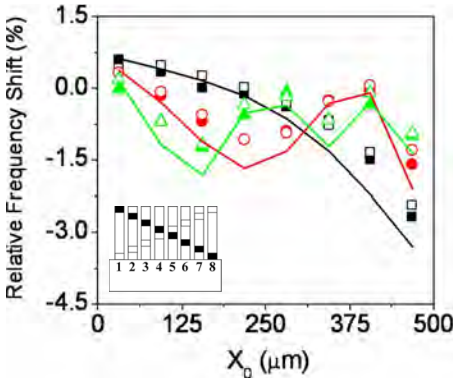


FIG. 7. (Color online) Relative frequency shifts for the first three modes as a function of the center position ($X_0$) for eight pieces of imaginary gold rectangles (62.5 $\mu$m long by 100 $\mu$m wide) derived from area differences of gold patterns on each neighboring cantilever in type C (solid rectangles) and type D (open rectangles): first (black squares), second (red circles), and third (green triangles). The colored lines represent theoretical calculations. The schematic depicts the dimensions and positions of the gold rectangles.

flexural rigidity. As the distance between the gold coating and the free end region increases for type C [Fig. 6(a)], the frequency decreases (cantilevers 1–5) until the flexural rigidity effect overrides the mass effect. In contrast, as the distance between the coating and the clamping region increases for type D [Fig. 6(b)], the frequency increases (cantilevers 1–4) until the mass effect overrides the flexural rigidity effect. The coating distances at the minimum and maximum fundamental resonance frequency shifts in Figs. 6(a) and 6(b) are 312.5 and 250 $\mu$m, respectively, which are close to the zero crossover position observed in Fig. 5(a) ($X_0 = \sim 190$ $\mu$m). From this observation, we determined that the gold coating distance giving the maximum response of the flexural rigidity effect is $\sim 200$ $\mu$m from the clamping region. As long as the evaporated materials are uniformly deposited onto the cantilever, the maximum positive fundamental frequency shift will be achieved. On the other hand, if the materials are uniformly deposited at a distance of $\sim 300$ $\mu$m from the free end region, the maximum negative fundamental frequency shift will be observed. As expected, the larger the area of the patterned gold coating, the larger the frequency decrease in the second and third modes.

To confirm the reliability and reproducibility of the relative frequency shifts in Figs. 5 and 6, we generated the gold patterns used in type A derived from area differences of gold patterns used in each type C and D cantilever. For example, the gold pattern on cantilever 2 of the type A array was derived from the area difference between cantilever 2 and cantilever 1 in type C. The schematic in Fig. 7 depicts the dimensions and positions of gold rectangles derived from type C (solid rectangles) and type D (open rectangles). Figure 7 shows the relative frequency shifts in the first three modes versus the position of the gold rectangles derived from type C (solid symbols) and type D (open symbols). The experimental data were compared to theoretical results (lines). The relative frequency shifts in Fig. 7 were similar to the frequency responses in Fig. 5, which confirms that the frequency shift data in Figs. 5 and 6 are reliable and reproducible.

## IV. CONCLUSIONS

In summary, we describe a reliable and systematic method to study the variations in bending profiles and frequency responses of cantilevers that have been treated with gold coatings that vary in position and area. Changes in the position and area of the partial gold patterns on the cantilevers were reflected in the local bending profiles, slope, and local curvatures because the gold patterns produced various types of bending profiles. The same length of partial gold patterns induced parallel bending profiles of the cantilevers because the same curvature was present at the gold coated region. The sum of each bending profile of the equally divided patterns was similar to the bending profile of the fully gold coated cantilever.

In addition, we observed that changes in the frequency modes were determined by the position and area of the gold film because the mass and the flexural rigidity had opposite effects on the resonance frequencies. We also determined the highest and lowest sensitivity of mass and flexural rigidity by using frequency shifts in the increasing gold patterns from the free end or clamping region. To elucidate how the frequency shifts vary with the position and area of the gold, the experimental harmonic frequencies were compared to the results of a theoretical one-dimensional model and FEM. Both the theoretical model and the simulation showed trend curves that were similar to the experimental data. These results provide information that can be used to improve the sensitivity and reproducibility of both deflection and frequency measurements and can be extended to other adsorbates including biological and chemical molecules.

## ACKNOWLEDGMENTS

This work was supported by the Korea Science and Engineering Foundation (KOSEF) grant funded by the Korea government (R01-2007-000-10882-0). S.K. and T.T. would like to acknowledge the partial support from the ORNL Bioenergy Science Center. Oak Ridge National Laboratory is managed by UT-Battelle, LLC for the U.S. Department of Energy under Contract No. DEAC05-00OR22725. D.L. and S.K. equally contributed to this work.

[1] J. Fritz, M. K. Baller, H. P. Lang, H. Rothuizen, P. Vettiger, E. Meyer, H. J. Guntherodt, C. Gerber, and J. K. Gimzewski, Science **288**, 316 (2000).
[2] T. Thundat, R. J. Warmack, G. Y. Chen, and D. P. Allison, Appl. Phys. Lett. **64**, 2894 (1994).
[3] P. A. Rasmussen, O. Hansen, and A. Boisen, Appl. Phys. Lett. **86**, 203502 (2005).
[4] M. Alvarez and J. Tamayo, Sens. Actuators B **106**, 687 (2005).
[5] T. Thundat, P. I. Oden, and R. J. Warmack, Microscale Thermophys. Eng. **1**, 185 (1997).
[6] R. Raiteri, M. Grattarola, H.-J. Butt, and P. Skládal, Sens. Actuators B **79**, 115 (2001).
[7] G. Y. Chen, T. Thundat, E. A. Wachter, and R. J. Warmack, J. Appl. Phys. **77**, 3618 (1995).
[8] D. Ramos, J. Tamayo, J. Mertens, M. Calleja, and A. Zaballos, J. Appl. Phys. **100**, 106105 (2006).
[9] D. Ramos, M. Calleja, J. Mertens, A. Zaballos, and J. Tamayo, Sensors **7**, 1834 (2007).
[10] D. Ramos, J. Tamayo, J. Mertens, M. Calleja, L. G. Villanueva, and A. Zaballos, Nanotechnology **19**, 035503 (2008).
[11] J. Tamayo, D. Ramos, J. Mertens, and M. Calleja, Appl. Phys. Lett. **89**, 224104 (2006).

[12]G. Wu, R. H. Datar, K. M. Hansen, T. Thundat, R. J. Cote, and A. Majumdar, Nat. Biotechnol. **19**, 856 (2001).
[13]S. Jeon, N. Jung, and T. Thundat, Sens. Actuators B **122**, 365 (2007).
[14]J. Mertens, M. Calleja, D. Ramos, A. Tarýn, and J. Tamayo, J. Appl. Phys. **101**, 034904 (2007).
[15]M. Godin, P. J. Williams, V. Tabard-Cossa, O. Laroche, L. Y. Beaulieu, R. B. Lennox, and P. Grütter, Langmuir **20**(17), 7090 (2004).
[16]V. Tabard-Cossa, M. Godin, I. J. Burgess, T. Monga, R. B. Lennox, and P. Grütter, Anal. Chem. **79**, 8136 (2007).
[17]S. Jeon and T. Thundat, Appl. Phys. Lett. **85**, 1083 (2004).
[18]J. Mertens, M. Álvarez, and J. Tamayo, Appl. Phys. Lett. **87**, 234102 (2005).
[19]M. Helm, J. J. Servant, F. Saurenbach, and R. Berger, Appl. Phys. Lett. **87**, 064101 (2005).
[20]R. Sandberg, K. Mølhave, A. Boisen, and J. Wsvendsen, J. Micromech. Microeng. **15**, 2249 (2005).